ACES Asian Chemical Editorial Society

doi.org/10.1002/asia.202401162

CHEMISTRY AN ASIAN JOURNAL Research Article

www.chemasianj.org

Homobimetallic Ruthenium(II) Complexes Catalysed Selective Transfer Hydrogenation of Aldehydes in Water

Gopal Deshmukh,[a] Thakur Rochak Kumar Rana,[a] Gopalan Rajaraman,*[a] and Ramaswamy Murugavel*[a]

Dedicated to Prof. Hiriyakkanavar Ila on the occassion of her 80th birthday

Herein we report chemoselective transfer hydrogenation (TH) of aldehydes in aqueous medium using a series of homobimetallic Ru(II) catalysts. Two homobimetallic complexes (**Ru1** and **Ru3**) and one monometallic complex (**Ru2**) have been employed in the catalytic reduction of aldehydes. Bimetallic complex [(*p*-cymene)$_2$(RuCl)$_2$L^3] (**Ru3**) is obtained from the reaction of Schiff base ligand 2,2′-((1E,1′E)-((3,3′,5,5′-tetraisopropyl-[1,1′-biphenyl]-4,4′diyl)bis(azaneylylidene))bis(methaneylylidene))bis(4-bromophenol) (**H$_2$L^3**) and characterized by various spectroscopic and analytical techniques. The use of formic acid/formate buffer as the hydride source and a catalyst loading of 0.01 mol% of **Ru1** or **Ru3** resulted in the conversion of various aldehydes to the corresponding alcohols in good to excellent yield. This method is very efficient for selective reduction of aldehydes in the presence of other reducible functional groups. A loading of 0.0001 mol% of **Ru1** catalyst is sufficient to achieve a turnover frequency (TOF) of 5.5×10^5 h^{-1}. Furthermore, the catalyst can been recycled and reused for six consecutives cycles without sacrificing the efficiency. A comparison of results obtained between bimetallic and monometallic complexes offers valuable insights into the distinct reactivity patterns of the bimetallic complexes, presumably originating from a cooperative effect. To understand the detailed mechanism, we have explored the mechanistic pathway using DFT methods on reported catalysts and various models which indicate that addition of aldehyde as rate-limiting and presence of cooperativity that boost the catalytic efficiency in the case of dinuclear **Ru1** catalyst. The pH dependent TH mechanism has been investigated with the aid of NMR and ESI-MS spectroscopic techniques.

Introduction

Alcohols are precursors for various organic transformations and can be obtained by the reduction of carbonyl compounds using a variety of methods.[1] Conventionally, many alcohols are obtained from carbonyl compounds by using reducing agents such as borohydrides, silanes or by transition metal catalysts under high pressure of hydrogen gas.[2–5] However, hydrogenation using molecular H_2 not only requires sophisticated instrumental setup but also has its own safety concerns. In the recent past, transition metal-catalyzed transfer hydrogenation (TH) for the production of alcohols has gained significant attention due to its recognized selectivity and versatility under mild conditions.[6–9] Specifically, TH is a promising alternative to traditional reduction methods comprising of Mn, Fe, Co, Ru, Rh, Ir and Pd-based homogeneous and heterogeneous catalysts.[9–16] Majority of the known approaches for hydrogenation reactions use isopropanol or H_2 gas as the hydride source in an organic solvent medium.[3,4] However, owing to increasing concerns on environmental and ecological issues, TH of carbonyl compounds in water is greatly preferred, because of its green-chemistry characteristics. In this context, TH of carbonyl compounds has been investigated earlier by employing formic acid or formate buffer as the hydride source and using water as the solvent or reaction medium (Scheme 1).[7,17–22]

Water mediated TH received much attention since the report of Xiao and co-workers using iridium catalyst for reduction of ketones.[20,22,23] Furthermore, TH of ketones in water or water-containing reaction mixtures, employing Ru, Rh, and Ir based catalysts with improved catalyst efficiency has been established, including for enantioselective reactions.[19–21,24] Seminal work on TH was reported by Tang and co-workers for the reduction of carbonyl groups in water using water a soluble iridium catalyst that is known now as 'Tang's catalyst'. Using this catalytic system, aldehydes and ketones were reduced chemoselectively in high yield using formic acid as the hydride source (Scheme 1).[25–27] Despite the advancement achieved with Xiao's and Tang's catalysts for the selective TH reactions, these catalysts were not recovered. The ability to recycle and reuse the catalyst enhances the sustainability and economic viability of the catalytic processes. Thus, there has been a pressing need to design new molecular catalysts that can efficiently perform TH reactions under green conditions while maintaining the efficiency over multiple reaction cycles.

Thus, high catalyst loading of those catalysts made from expensive metals such as iridium, use of organic solvents, use of

[a] G. Deshmukh, T. R. K. Rana, G. Rajaraman, R. Murugavel
Department of Chemistry, Indian Institute of Technology Bombay, Powai, Mumbai 400076, India
E-mail: rmv@chem.iitb.ac.in
rajaraman@chem.iitb.ac.in

Supporting information for this article is available on the WWW under https://doi.org/10.1002/asia.202401162

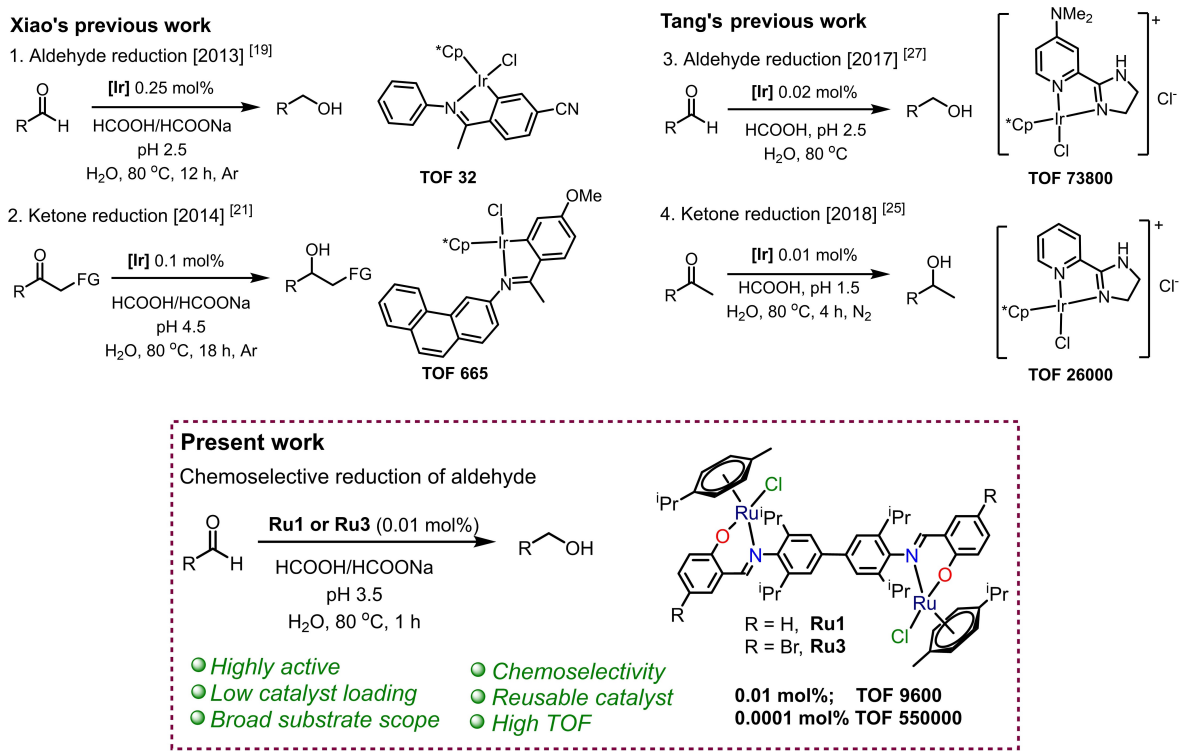

Scheme 1. Monometallic and bimetallic catalysts for transfer hydrogenation.

hazardous H_2 as a hydrogen source, lack of chemoselectivity, low green metrics, reusability and durability remain as challenges in this field.[9] One way to tackle such a convoluted combination of challenges would be to design water insoluble catalyst systems that can operate in an aqueous medium and utilize formate buffer as a hydride source and still exhibit high selectivity and reusability over multiple cycles for the alcohol production via TH.

Bimetallic catalysts have been shown to exhibit significant increase in both selectivity and reaction rate in metal catalyzed reactions compared to their monometallic counterparts.[28–40] A large number of examples of bimetallic catalysts have been reported in the literature for various organic transformations, such as hydroelementation of alkynes,[28] disproportionation of formic acid to methanol,[29] hydroamination,[30] hydroformylation,[31] TH for ketones[32] and propargylic reduction[33] and substitution[34] reactions. Yu and co-workers have reported bimetallic Ru-pincer complexes for homogenous TH of ketones using isopropanol as a hydride source and also demonstrated that a bimetallic complex is more active than the corresponding monometallic catalyst.[35,36] We have recently reported a novel bimetallic Ru(II) Schiff base catalyst for reductive amination (RA) reaction in water,[37] for one pot quinoline synthesis,[38] for β-alkylation of secondary alcohol[39] and microwave assisted hydrogenation.[40] These studies have shown that bimetallic complexes are more efficient than their monometallic counterparts.

In view of the above outlined merits and demerits of previously reported TH reactions, we have investigated in the present study a series of homobimetallic catalysts for chemoselective TH of aldehyde in water (Figure 1). In addition, comparison of their catalytic activity with that of the monometallic analogue **Ru2** is also presented.

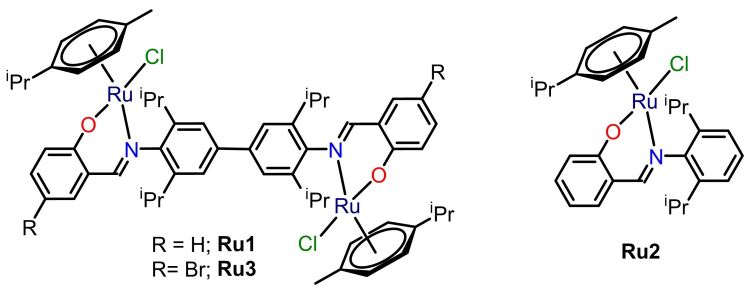

Figure 1. Bimetallic and monometallic catalysts employed for TH reaction.

Results and Discussion

Synthesis of H_2L^3 Ligand and Complex [(*p*–cymene)$_2$(RuCl)$_2L^3$] (Ru3)

We reported binuclear **Ru1** and mononuclear **Ru2** complexes as catalysts for one-pot reductive amination (RA).[37] **Ru1**, featuring a pseudo-C_2-symmetric N,O-donor ligand, demonstrated higher efficiency at lower loadings for secondary amine synthesis than its mononuclear analogue, **Ru2**. To further tune the steric and electronic properties of the ligand, we designed a new Schiff base ligand, H_2L^3, by condensing 5-bromosalicylaldehyde with 2,2′,6,6′-tetraisopropylbenzidine (TIBZ) in the presence of catalytic formic acid. Complex **Ru3** was synthesized by reacting H_2L^3 dipotassium salt with [Ru(*p*-cymene)(μ-Cl)Cl]$_2$, yielding dark red crystals through recrystallization from a dichloromethane:methanol solvent mixture (5:1 v/v), under ambient conditions (Scheme 2).

In the FT-IR spectrum of H_2L^3, the imine (–N=CH–) stretching band is observed at 1628 cm^{-1}, while a broad band around 3380 cm^{-1} corresponds to the phenolic -OH group, which disappears upon metalation (Figure S1). The imine stretch shifts to 1611 cm^{-1} in the **Ru3** complex, confirming the formation of the Ru–N=CH– bond. ESI-MS analyses show molecular ion peaks at m/z 719.166 ([M + H]$^+$) for H_2L^3 and 1223.150 for **Ru3** ([M–Cl]$^+$), supporting product formation (Figures S2 and S3). The NMR spectra reveal distinct resonances for the salicylaldimine group in H_2L^3 and confirm the presence of substituents in **Ru3**, consistent with the proposed structures. The proton NMR spectrum of H_2L^3 shows resonances for the salicylaldimine group at δ 8.31 ppm (–N=CH–) and δ 13.14 ppm (–OH) (Figures S4 and S5). In **Ru3**, six doublets for –CH(CH$_3$)$_2$ appear at δ 1.14–2.0 ppm, along with three septets and four doublets for p-cymene phenyl protons (Figure S6). ^{13}C NMR spectral signals observed are consistent with the structure of the desired products (Figure S7). The UV-vis spectra of H_2L^3 and **Ru3** in dichloromethane show intense intra-ligand transitions at 234, 271, and 348 nm for H_2L^3. In **Ru3**, bands at 230 and 266 nm indicate intra-ligand transitions, while the 448 nm band corresponds to a d$\pi\rightarrow\pi^*$ metal-to-ligand charge transfer (Figure S8).[37,38]

The molecular structures of H_2L^3 and **Ru3** are shown in Figure 2. In H_2L^3, the imine (–N=CH) bond distance N(1)-C(7) is 1.275 (3) Å (Figure 2a) and C(7)-N(1)-C(8) bond angle is 121.0 (2)°. In the molecular structure of H_2L^3, the binding sites are positioned in a trans orientation to each other. The diffraction quality of **Ru3** was poor, in spite several repeated measurements, and the best possible refined structure is shown in Figure 2b. In the molecular structure of **Ru3**, each of the ruthenium centers adopts an approximate piano-stool type coordination geometry (coordinated to the nitrogen atom of imine, phenoxide oxygen, chloride ion, and *p*-cymene moiety in an η^6 fashion. The Ru – N (2.113(7) Å) and Ru – O (2.072(7) Å) bond lengths are comparable to those reported in the literature.[37,41] The two phenyl rings of the central benzidine moiety in **Ru3** exhibit a twist angle of 31.2°, whereas the ligand H_2L^3 does not show any twist at all. Selected bond lengths and bond angles, crystal data and structure refinement for H_2L^3 is listed in Tables S2 and S3.

Catalytic TH of Aldehydes

We have explored the catalytic TH reaction using benzaldehyde (**1a**) as the model substrate and bimetallic **Ru1** as catalyst to produce benzyl alcohol (**2a**). The effect of pH on the TH of carbonyls and quinolines has been previously studied by the groups of Xiao and Tang.[19,22,25,27,42] Their results suggest that the formation of active catalyst is facilitated at a particular pH value. The pH value of the aqueous formic acid/formate buffer plays a significant role in the activity of the **Ru1** (Figure 3a). The reaction was probed with aqueous buffer solutions in the pH range of 5.0–2.5 (Table 1, Entries 1–15, Figure 3a). To prepare 100 mL of a 1 M HCOONa:HCOOH buffer solution with pH 3.5, we used 6.8 g of sodium formate (100 mmol) and 3.7 mL of formic acid (98–100% w/w, 100 mmol) dissolved in 96 mL of

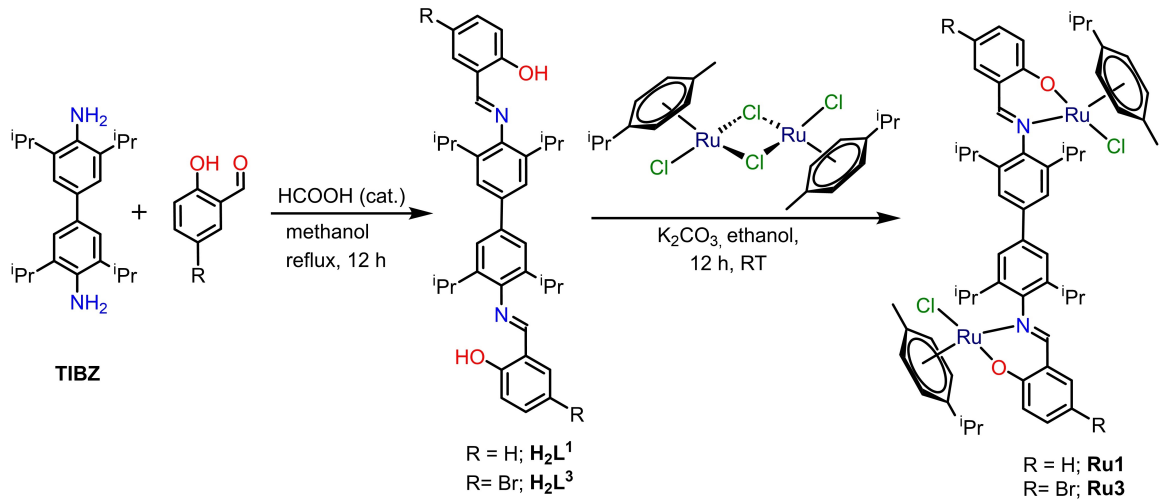

Scheme 2. Synthesis of **Ru1**[37] and **Ru3**.

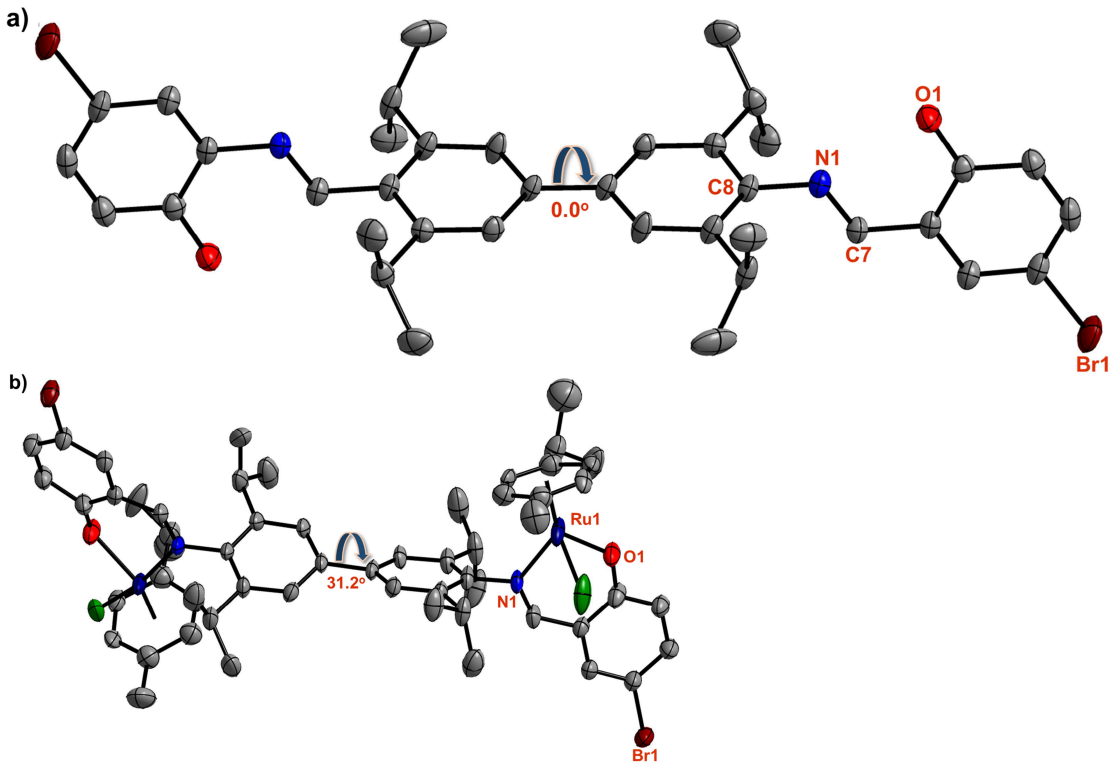

Figure 2. a. Molecular structure of H_2L^3 drawn at a 50% probability level for the thermal ellipsoids. Hydrogen atoms and solvent molecules are omitted for clarity. Selected bond lengths (Å) and bond angles (°) for H_2L^3: Br1-C(4); 1.901 (2), O(1)-C(1); 1.348 (3), N(1)-C(8); 1.425 (3), N(1)-C(7); 1.275 (3), C(7)-N(1)-C(8); 121.0 (2), O(1)-C(1)-C(6); 121.8 (2), O(1)-C(1)-C(2); 118.5 (2). **b**. Molecular structure of **Ru3** from a poorly refined diffraction data.

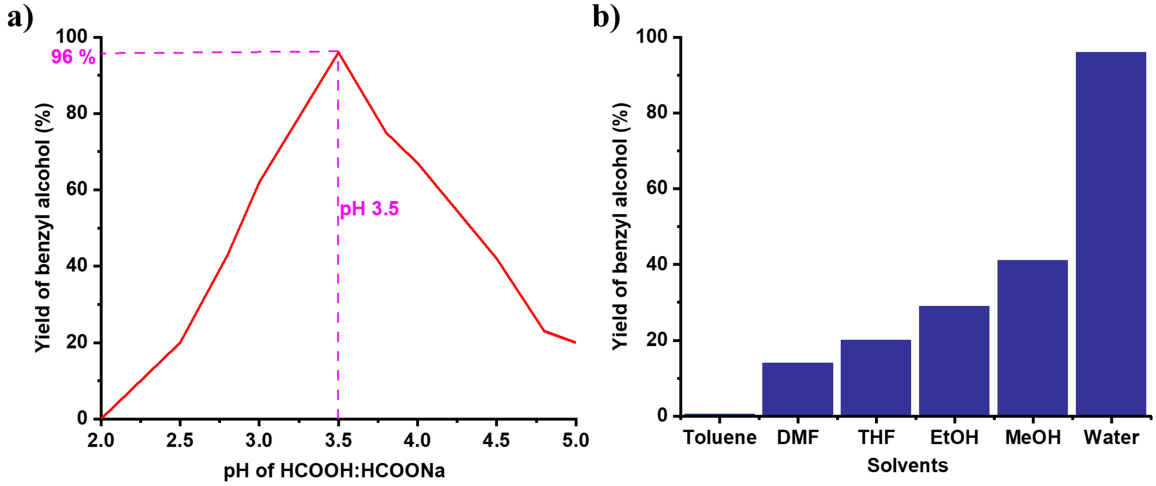

Figure 3. Plots of yield of formation of benzyl alcohol versus a) pH values employed in the reaction and b) change in solvents.

water. A 1 M formate buffer (3 mL) was used for 1 mmol of aldehyde, giving a buffer-to-aldehyde ratio of 6:1.

The catalyst, **Ru1**, exhibits the highest catalytic activity at pH 3.5 (formic acid/formate buffer); however, its efficiency drastically diminishes at both higher and lower pH values.

The decrease in catalyst performance at a high pH is attributed to decrease in the concentration of active catalyst intermediate species due to decomposition of formate ion (into CO_2 and HCO_3^-), reducing the formation of Ru-formate species. At low pH, Ru-hydride (active catalyst species) reacts with either protons in the reaction mixture or substrate aldehyde.[19] Thus, for the TH reaction, maximum benzyl alcohol formation was observed at pH 3.5. Similarly, at 80 °C the present catalytic system is more efficient compared to other earlier reported methods.[9] Optimization of catalyst loading showed that 0.01 mol% of **Ru1** is sufficient to get 96% yield of **2a** with a TON of 9600 (Table 1, Entries 1–7). However, the formation of **2a** reduced when the catalyst loading was lowered from 0.01 mol% to 0.0001 mol% (Table 1, Entries 8–10).

Table 1. Optimization of reaction conditions for transfer hydrogenation.

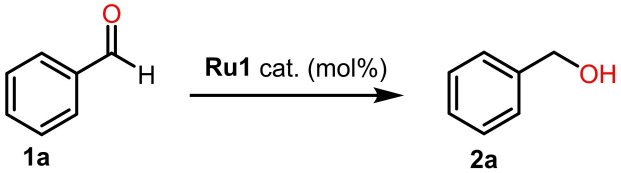

1a 2a

Entry	Cat. (mol%)	Solvent	Temp (°C)	Additive	pH	Time (h)	Yield (%)	[a]Con. (%)	TON	TOF (h^{-1})
1	0.2	H_2O	80	HCOONa:HCOOH	5.0	6	20	30	100	17
2	0.2	H_2O	80	HCOONa:HCOOH	4.8	6	23	29	115	20
3	0.2	H_2O	80	HCOONa:HCOOH	4.5	6	42	52	210	35
4	0.2	H_2O	80	HCOONa:HCOOH	4.0	3	67	70	335	112
5	0.2	H_2O	80	HCOONa:HCOOH	3.8	3	75	78	375	125
6	0.02	H_2O	80	HCOONa:HCOOH	3.3	3	89	93	4450	1483
7	**0.01**	**H_2O**	**80**	**HCOONa:HCOOH**	**3.5**	**1**	**96**	**100**	**9600**	**9600**
8	0.001	H_2O	80	HCOONa:HCOOH	3.5	1	83	90	83000	83000
9	0.0001	H_2O	80	HCOONa:HCOOH	3.5	1	55	59	550000	550000
10	0.0005	H_2O	80	HCOONa:HCOOH	3.5	1	68	70	136000	144000
11	0	H_2O	80	HCOONa:HCOOH	3.5	3	NR	-	-	-
12	0.01	H_2O	80	-	3.5	2	NR	-	-	-
13	0.1	H_2O	80	HCOONa:HCOOH	3.0	6	62	72	620	12
14	0.1	H_2O	80	HCOONa:HCOOH	2.8	6	43	48	430	72
15	0.1	H_2O	80	HCOONa:HCOOH	2.5	6	20	25	200	33
16	0.1	MeOH	70	HCOONa:HCOOH	3.5	6	41	49	410	68
17	0.1	EtOH	90	HCOONa:HCOOH	3.5	12	29	12	290	24
18	0.1	Toluene	100	HCOONa:HCOOH	3.5	12	NR	-	-	-
19	0.1	DMF	120	HCOONa:HCOOH	3.5	12	14	18	140	12
20	0.1	THF	100	HCOONa:HCOOH	3.5	12	20	25	200	17
21	1	^{i}PrOH	80	KOH	-	12	53	57	53	4.5

Reaction conditions: benzaldehyde (1 mmol), solvent (2 mL), HCOONa:HCOOH (3 mL), [a]conversions of benzaldehyde was monitored using GC-MS.

The model reaction using **Ru1** as a catalyst was performed with various organic solvents such as methanol, ethanol, toluene, dimethylformamide (DMF) and tetrahydrofuran (THF) in the presence of aqueous buffer solution (pH 3.5 of HCOONa:HCOOH). However, these organic solvents resulted in poor efficiency for the formation of **2a**. Water as the reaction medium showed an increase in the efficiency (Table 1, Entries 16–20, Figure 3b). **Ru1** is highly soluble in most of the organic solvents, which hampers the reusability of catalyst. Thus, the optimal reaction conditions for TH are 0.01 mol% **Ru1** as a catalyst, at pH 3.5 using HCOONa:HCOOH buffer as the hydride source in water at 80 °C for 1 hour.

Catalyst screening was carried out at optimal reaction conditions using formate buffer at a pH of 3.5 at 80 °C in water. Use of 0.01 mol% of both **Ru1** and **Ru3** showed excellent activity towards the reduction of benzaldehyde. (Table 2, Entries 1–3). In contrast, 0.02 mol% monometallic catalyst **Ru2** gave a lower yield (40%) of **2a** under similar conditions. When the catalyst loading of **Ru2** was increased even up to 1 mol%, **2a** was obtained only in 59% yield (Table 2, Entries 4 and 5). Thus, an apparent cooperativity between the two ruthenium centers gives better TH yields in case of bimetallic catalysts **Ru1** and **Ru3**, as has been demonstrated earlier for reductive amination of aldehydes in water using similar catalysts.[37] Reactions carried out using the Ru-precursor complex [Ru(*p*-cymene)(μ-Cl)Cl]$_2$ did not produce the desired product (Table 2,

Table 2. Screening of catalyst for transfer hydrogenation.

Entry	Catalyst	Catalyst loading (mol%)	Time (h)	Yield of **2a** (%)	Conversion (%)
1	**Ru1**	0.01	1	96	100
2	**Ru3**	0.01	1	93	100
3	**Ru3**	0.01	1.3	98	100
4	**Ru2**	0.02	1	40	46
5	**Ru2**	1	3	59	64
6	[Ru(*p*-cymene)Cl$_2$]$_2$	0.01	6	NR	-

Reaction conditions: benzaldehyde (1 mmol), HCOONa:HCOOH (3 mL, pH 3.5), water (2 mL), 80 °C for 1 h, conversion was monitored using GC-MS.

Entry 6). Thus, the conditions of pH = 3.5 is more suitable for the **Ru1** than **Ru2** as observed from the optimization of reactions conditions.

Using as the above optimised conditions, the substrate scope for various aldehydes was explored as shown in Scheme 3. The benzaldehydes with electron-donating substituents such as methyl and methoxy delivered desired benzyl alcohols **2b**–**2f** in >90% yield. Electron-withdrawing substituents such as nitro, cyano, and trifluoromethyl on the aromatic ring are efficiently reduced to the corresponding benzyl alcohols **2h** (99%), **2i** (98%), and **2k** (96%). Similarly, the halo substituted benzaldehydes produce the corresponding aromatic alcohols in high yield (**2l**; 92%, **2m**; 90%, **2n**; 91%, **2o**; 94%, **2p**; 93%, **2q**; 91%, **2r**; 93%). The disubstituted benzaldehydes were successfully reduced to corresponding benzyl alcohols **2g** (98%) and **2s**–**2u** (95–96%), in high yields. Aliphatic and heterocyclic aldehydes were reduced easily to afford desired products **2v** (93%), **2w** (84%), **2x** (91%), **2y** (89%), **2z** (83%).

As shown in Scheme 4, under optimal reaction conditions, special attention has been given to the chemoselective reduction of unsaturated aldehydes. Catalyst **Ru1** exhibited high chemoselectivity for hydrogenation of substrates such as cinnamaldehyde and 3,4-methoxy cinnamaldehyde, affording corresponding unsaturated alcohols **4a** (91%) and **4b** (88%) in good yields, without affecting the alkene bonds. Similar behaviour was also observed for the reduction of 10-undecenal, citral and citronellal to selectively yield **4c** (86%), **4d** (88%), and **4e** (91%). Piperonyl alcohol **4f**, an anti-oxidant compound was selectively synthesized from piperonal in 94% yield using similar reaction conditions.

Further, experiments have been performed to emphasize the chemoselectivity between ketone (acetophenone) and aldehyde (benzaldehyde) (1:1 ratio) functional groups. As shown in Scheme 5, it was observed that only benzaldehyde gets reduced to benzyl alcohol and no conversion of acetophenone was observed. Compared to aldehydes, ketones experience greater steric hindrance, resulting in lower electrophilicity and reduced nucleophilicity. Additionally, under the optimized reaction conditions, the carbonyl group in ketones may not be adequately activated, resulting in no reduction. Thus, **Ru1** chemoselectively catalyses aldehyde to alcohol.

The efficiency of **Ru1** was measured in terms of TONs and TOFs for the TH reaction of benzaldehyde under optimal reaction conditions, which shows a TOF of 9600 h^{-1}. Additionally, the reaction was carried out using an exceptionally low

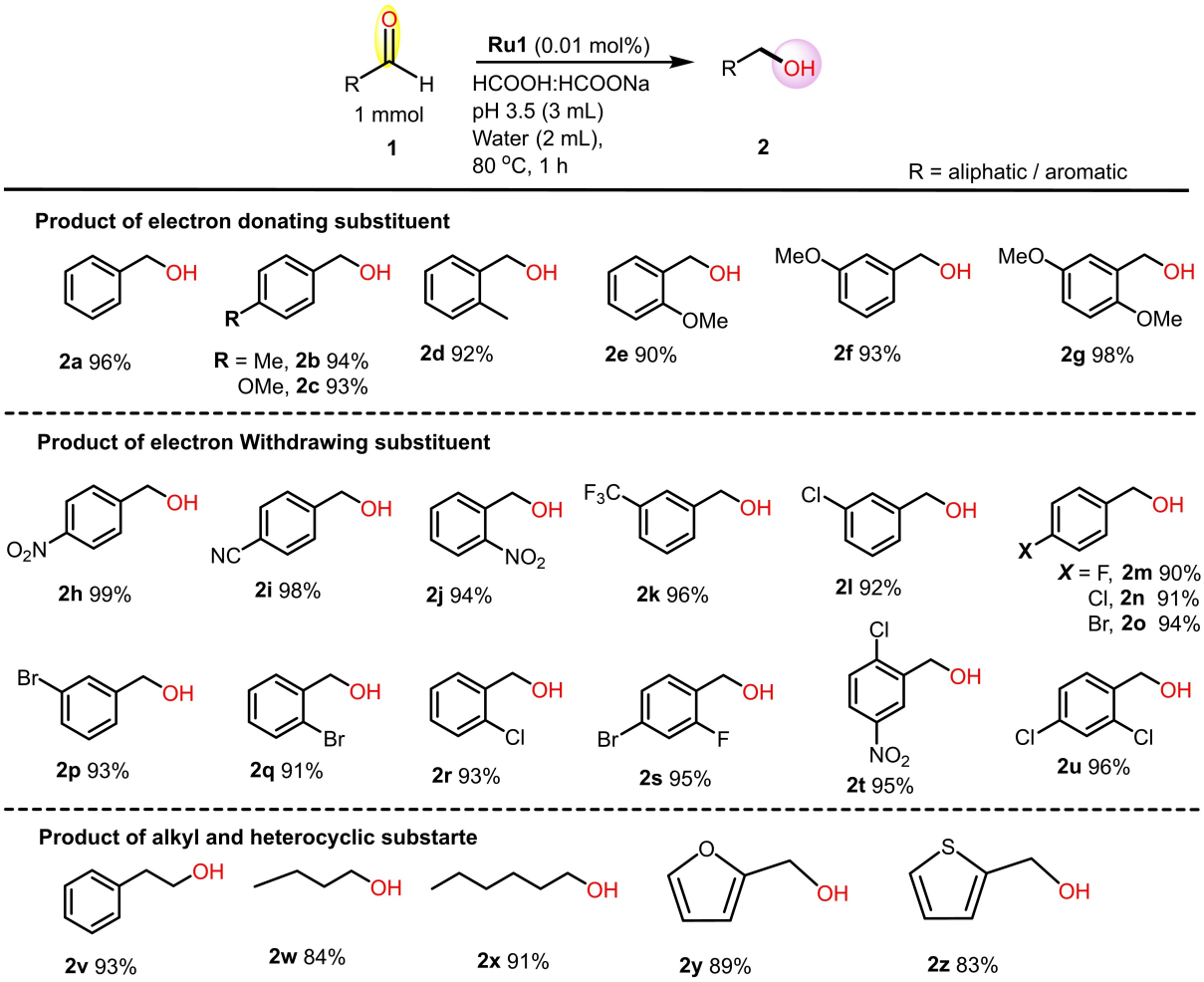

Scheme 3. Substrate scope for TH of aldehydes.

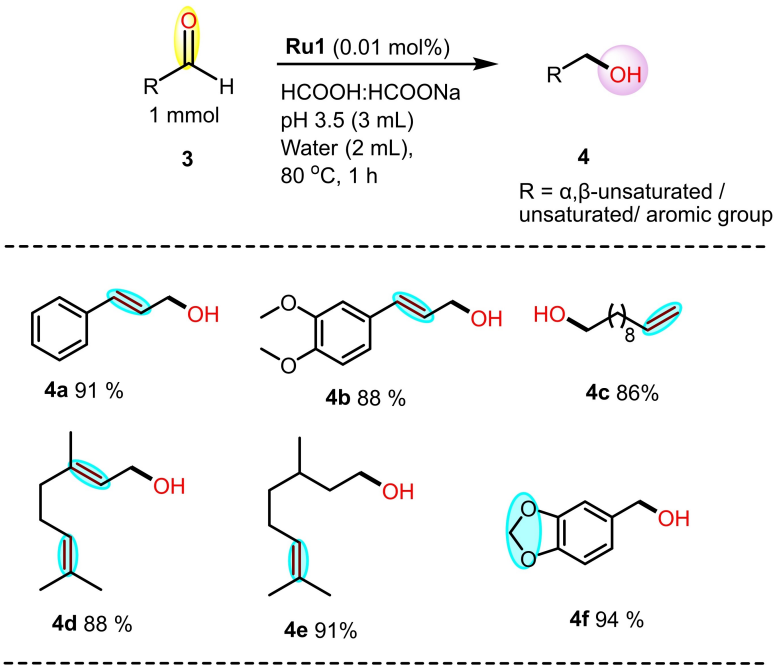

Scheme 4. Substrate scope for unsaturated aldehydes

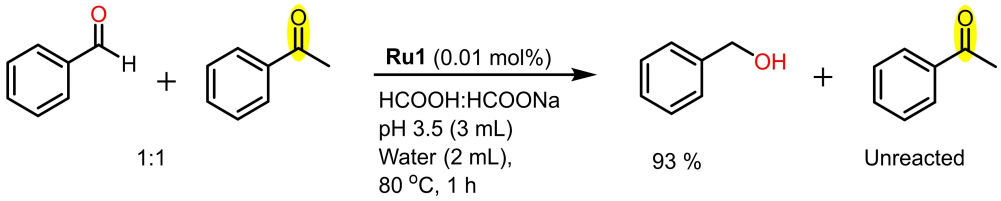

Scheme 5. Selectivity experiment between aldehyde and ketone.

catalyst loading of 0.0001 mol% (equivalent to 0.001 mg of **Ru1**), which resulted in a 55% yield of benzyl alcohol. Under these conditions, a remarkably high TON and TOF of 5.5×10^5 h^{-1} were observed, highlighting the outstanding efficiency and atom economy of the present catalytic system in water. The results underscore the significance of this catalyst, particularly in achieving high efficiency with minimal ruthenium loading (Figure S9). Analysis of green metrics for TH using **Ru1** catalyst showed high atom economy (98.14%), atom efficiency (94.21%) and reaction mass efficiency (98%) (Table S4).

The present **Ru1** based TH reaction can be easily scaled up. As shown in Scheme 6, 1.16 g (11 mmol) of benzaldehyde is reduced to 1.13 g of benzyl alcohol (95% yield) using 0.01 mol% of **Ru1** catalyst. This experiment coupled with the aforementioned TONs and TOFs demonstrate the practicality and high efficiency of **Ru1** catalysed TH reaction.

Comparative Study of Homobimetallic (Ru1 and Ru3) with Monometallic (Ru2) Catalyst

Comparison of the catalysis outcome and computational insights of ruthenium catalysts for reductive amination reaction has revealed the superiority of bimetallic catalyst over monometallic counterpart.[37,38] To evaluate the effect of cooperativity in bimetallic **Ru1** and **Ru3** (0.01%) vis-à-vis **Ru2** (0.02 mol%), a

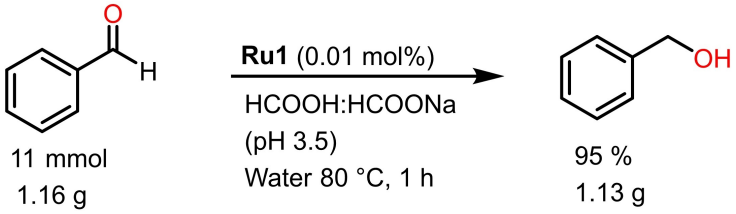

Scheme 6. Gram scale TH conversion of benzaldehyde.

Table 3. Comparison of homobimetallic **Ru1**/**Ru3** with monometallic **Ru2** complex.

Entry	Product	Yield (%)		
		Ru1 (0.01 mol%)	**Ru3** (0.01 mol%)	**Ru2** (0.02 mol%)
1	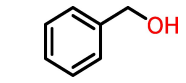	96	93	40 (73) [a]
2	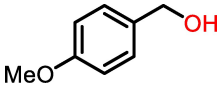	93	97	42
3	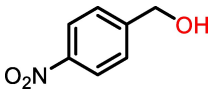	99	98	51
4	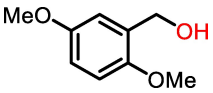	98	97	58
5	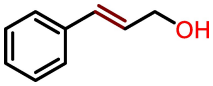	91	89	34

Reaction conditions: aldehyde (1 mmol), **Ru1**/**Ru3** (0.01 mol%) and **Ru2** (0.02 mol%), formic acid/formate buffer (3 mL, pH 3.5), water (2 mL), 80 °C for 1 h, isolated yield, [a] use of 2 mol% of **Ru2.**

range of substrates containing electron-donating (–OMe, 2,4-OMe) or electron-withdrawing (–NO_2 and α,β-unsaturated aliphatic aldehyde) substituents has been used. These substrates were found to exhibit similar reactivity patterns for **Ru1** and **Ru3** (Table 3). On the other hand, of the conversion efficiencies with **Ru2** complex was found to be considerably low (in spite of using 0.02 mol% of catalyst **Ru2**) (Table 3). A further increase in catalyst loading of **Ru2** (0.02 mol% to 2 mol%), could only increase the benzyl alcohol formation from 40% to 73% (Table 3). The pre-catalyst activation could be attributed to the cooperative interaction between two metals in **Ru1**/**Ru3**, which is absent in **Ru2**. In summary, TH catalytic conversion of benzaldehyde to benzyl alcohol by **Ru1** and **Ru3** has been substantially higher than **Ru2**. These catalysts do not affect the unsaturated C=C bonds as well as other functional groups on substituted aldehydes, leading to the formation of a range of substituted alcohols.

Kinetic studies were conducted to investigate the reactivity differences between the bimetallic catalyst **Ru1** and the monometallic catalyst **Ru2**. Parallel reactions with benzaldehyde were carried out using 0.01 mol% of **Ru1** and 0.02 mol% of **Ru2**, with product formation monitored at 10 minute intervals (Table 4). The results revealed distinct variations in rate of the reactions among the catalysts. The bimetallic catalyst **Ru1** initiated product formation within the first 10 minutes, achieving a ~33% yield of **2a**. In contrast, **Ru2** required almost 50 minutes to reach a similar yield of 34%. By the end of the reaction (1 hour), **Ru1** produced a 96% yield of **2a**, while **Ru2** achieved only 40% (Figure 4). The rate of the reactions calculated for each catalyst were: **Ru1**: $k = 0.321$ mM L^{-1} min^{-1} and **Ru2**: $k = 0.133$ mM L^{-1} min^{-1} (Table 4). These results indicate that bimetallic **Ru1** is 2.4 times more active and efficient than monometallic **Ru2** catalyst. The superior performance of the bimetallic catalysts can be attributed to enhanced electronic interactions between the two metal centres. These interactions significantly influence the catalyst's reactivity and play a crucial role in stabilizing key intermediates during the catalytic cycle.

Table 4. Kinetic study of the **Ru1 and Ru2** catalysts.

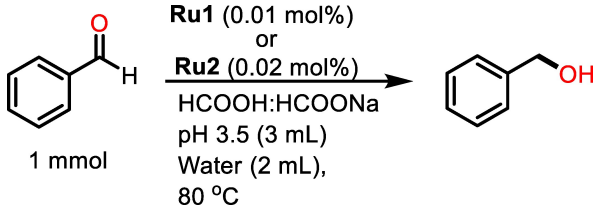

Entry	Time	Yield of benzyl alcohol (%)	
		Ru1	**Ru2**
1	0	0	0
2	10	33	3
3	20	59	11
4	30	78	19
5	40	87	27
6	50	95	34
7	60	96	40
Rate (mM L^{-1} min^{-1})		$k = 0.321$	$k = 0.133$

Catalyst Recycling

The **Ru1** catalyst is insoluble in the water, so the reduction is occur in heterogenous medium. Efforts have been made to recover the catalyst for reuse in subsequent reactions. After the catalytic reaction of benzaldehyde under the optimized reaction

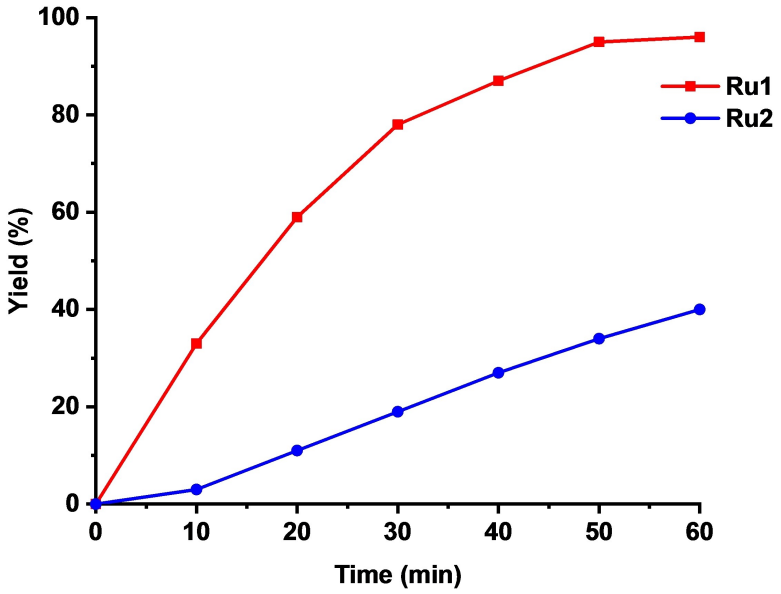

Figure 4. Plot shows the change in benzyl alcohol yield with respect to time for **Ru1** and **Ru2** catalysts.

conditions, the yield of **2a** obtained was 96% in the first cycle using 0.01 mol% (~0.22 mg for 2 mmol of benzaldehyde) of the **Ru1** catalyst. Subsequently, the catalyst was filtered off as residue and the product was extracted from the filtrate (Scheme S1). After the first catalytic run, the catalyst was reused for second cycle without further purification in the same reaction flask. For the next cycle, again 96% yield was obtained. Similarly, subsequent four additional catalytic runs were carried out, wherein the yields of **2a** obtained were 95%, 91%, 90% and 86%, respectively (Figure 5a). After the 6th catalytic run, the ESI-MS of the catalyst residue revealed the existence of Ru-formato species corresponding to $[M+Na]^+$ at *m/z* 1143.381 (Figures 5b and S10). These repetitive experiments suggests that the catalyst **Ru1** is robust and active over successive reaction cycles and can be reused several times.

Mechanism for Transfer Hydrogenation

The electronic structure of the optimized geometry of catalyst **Ru1** has already been reported in a previous study.[37] Based on the experimental findings described above and previously reported mechanisms for similar reactions, we have adopted the following mechanism for the transfer hydrogenation of aldehydes

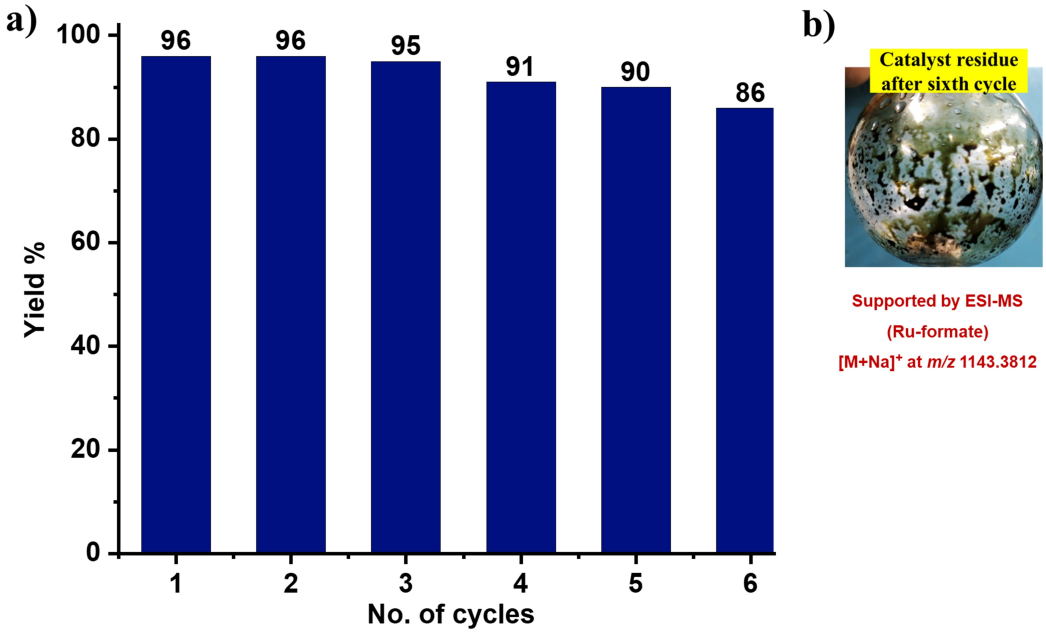

Figure 5. a) Reusability of **Ru1** for transfer hydrogenation and b) Picture of reaction vessel containing **Ru1** catalyst residue.

(Scheme 7).[19,25,27] In the first step, **Ru1** (species **I**) undergoes chloride ion exchange with formate ion, resulting in the formation of Ru-formate species **II** which is found to be exothermic by $-251.9\ kJ\,mol^{-1}$. This facile formation and large exothermic energy associated with its formation add to its stability and was confirmed by mass spectral analysis by analyzing the reaction mixture 10 min from the start of the reaction, which revealed the presence of a peak at *m/z* 1121.299 corresponding to the $[M+H]^+$ ion (Figure S11). Subsequently, after 15 min from the start of the reaction, species **II** undergoes β-hydride transfer through CO_2 elimination, resulting in ruthenium-hydride species **III**, the formation of which is found to be $21.3\ kJ\,mol^{-1}$ from species **II**, suggesting facile formation. This step is favoured by the proximity of the H atom of the formate to Ru (H···Ru at the species **II** is 2.979 Å) to enable the formation of Ru–H species. The formation of species **III** was also supported by ESI-MS spectrometry, revealing the presence of peak at *m/z* 1031.312 corresponding to $[M-H]^+$ ion (Figure S12).

In the next step, the aldehyde species are expected to coordinate with the Ru centers (species **IV**). For this coordination to occur, the linked nitrogen atom in the Schiff-base ligand undergoes dissociation, eventually resulting in the establishment of a potent η^2 bond with the C=O group of the aldehyde. As this involves cleavage of the Ru–N bond and the formation of the Ru η^2 (R–CH=O) bond, this is found to be endothermic from species **III** by $116.5\ kJ\,mol^{-1}$.

However, from the reactants, the formation is exothermic by $-113.7\ kJ\,mol^{-1}$. In the next step, hydride migration to the carbon atom of the coordinate aldehyde is expected, leading to the formation of species **V**, and this is facilitated at species **IV** with the short H···C(aldehyde) of 2.259 Å. The formation of species **V** is endothermic by $24.0\ kJ\,mol^{-1}$ from species **IV** as shown in Figure 6. In the next step, the oxygen atom of the coordinated aldehyde will be protonated from the acid buffer that is added in the reaction leading to the release of the product and the regeneration of the species **II** whose formation is also exothermic, suggesting a facile reaction. A similar pathway is followed when **Ru2** and **Ru3** was used as the catalyst (Figure 7 and Scheme S2). Both intermediate species for **Ru3** i.e. Ru-formate **II'** ($[M\text{-}OCOH]^+$ at *m/z* 1233.176) and Ru-hydride **III'** ($[M/2]^+$ at *m/z* 594.086) have been detected in ESI-MS spectra (Figures S13 and S14).

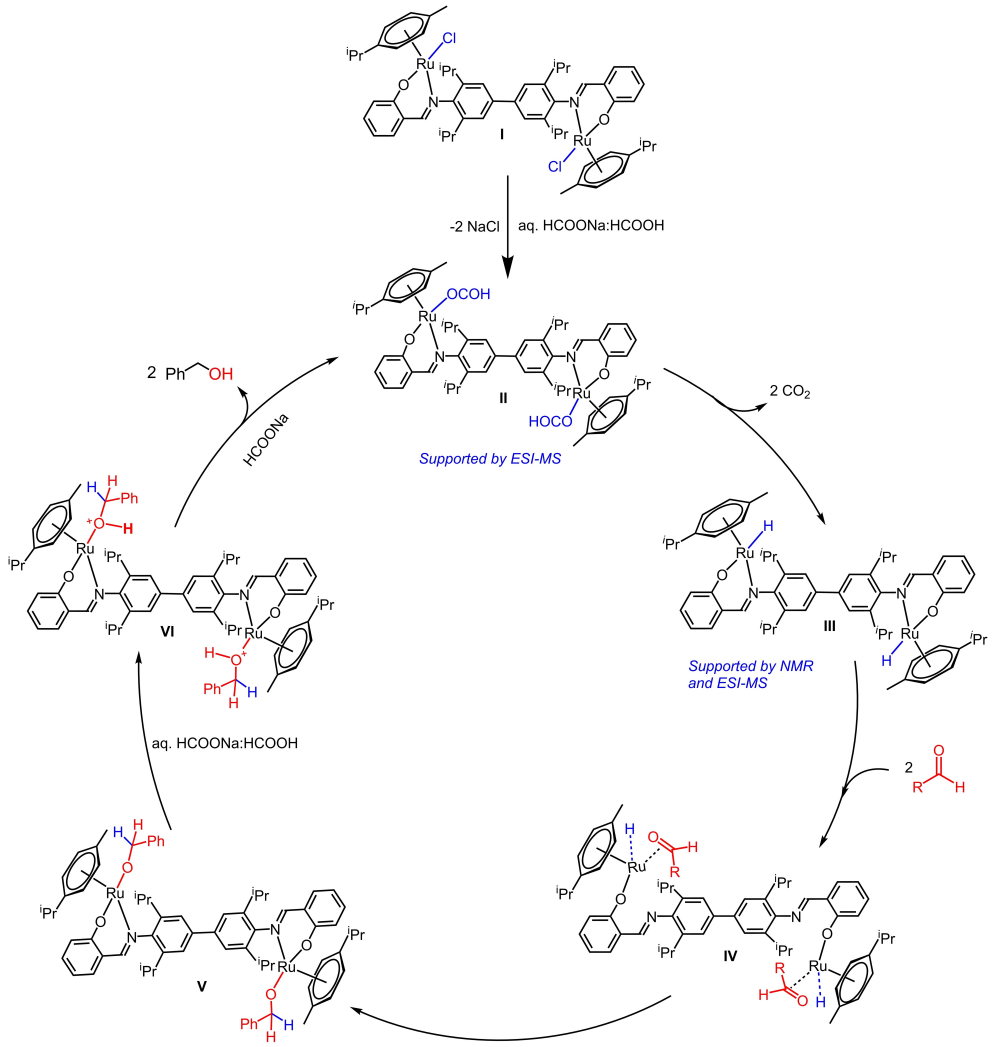

Scheme 7. Proposed catalytic cycle for transfer hydrogenation with **Ru1.**

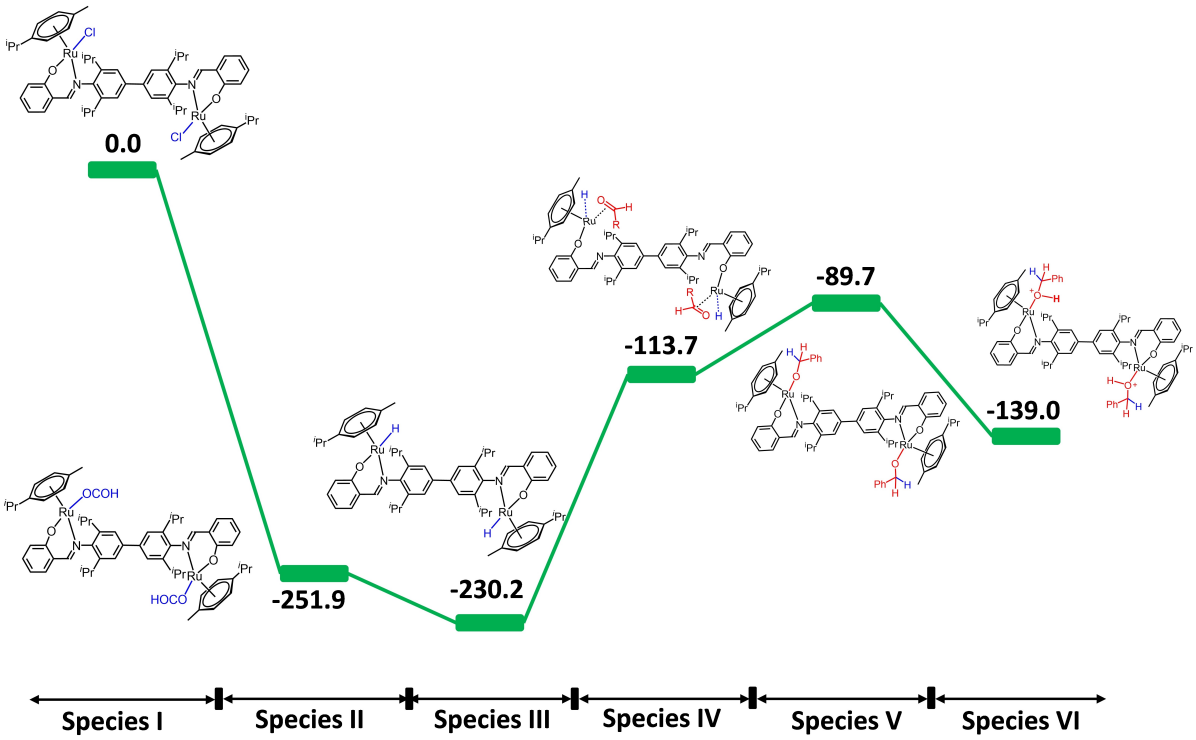

Figure 6. The computed potential energy profile diagram in solvent phase free energies (ΔG, kJ/mol), at the B3LYP–D3/def2-TZVP level of theory for reaction pathways of the bimetallic complex for species **I** to **VI.**

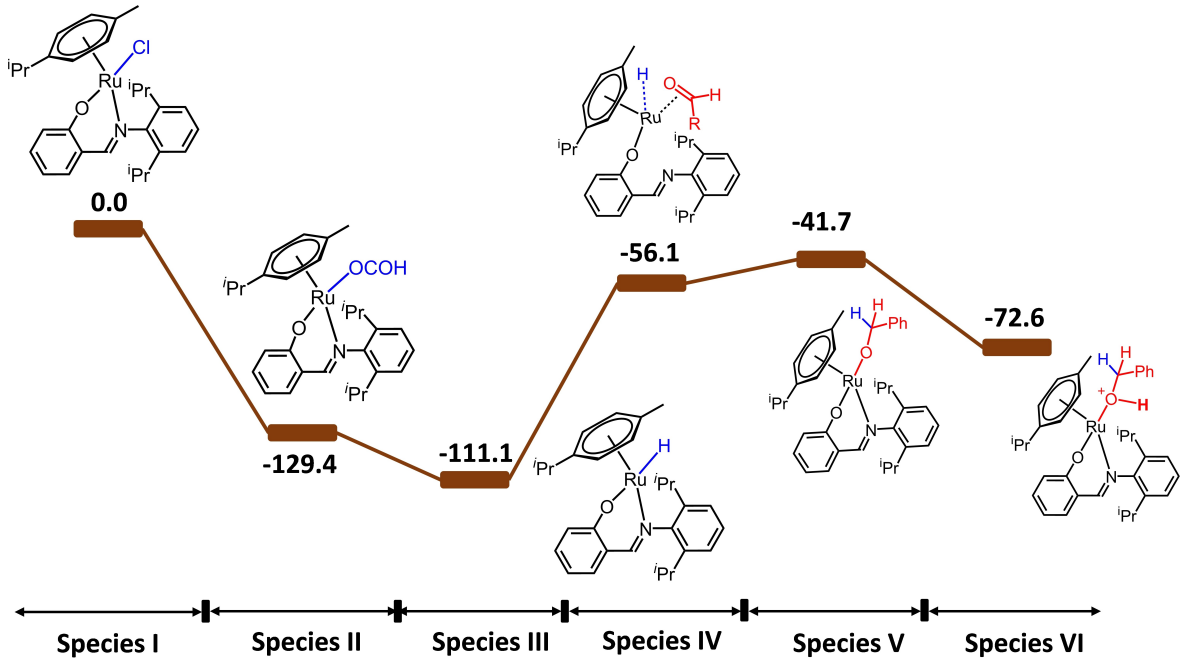

Figure 7. The computed potential energy profile diagram in solvent phase free energies (ΔG, kJ/mol), at the B3LYP–D3/def2-TZVP level of theory for reaction pathways of the monometallic complex for species **I** to **VI.**

To understand observed experimental rate for **Ru1** vis-à-vis **Ru2**, we have performed calculations for monometallic species also as shown in Figure 7 and the comparison of reactivity of one versus two metal centres for both catalysts, **Ru1** and **Ru2** also explored. It has also been observed that the computed reactivity pattern for **Ru1** has resulted in stability of each intermediate as clear from their larger exothermic energy of formation. Further statistical probability is also higher for the dimer since it contains two active metal centres. Experimentally,

reaction of transfer hydrogen to benzaldehyde is more for **Ru1**, 2.4 times more reactive than the **Ru2**.

The crucial step in the reaction mechanism that governs the kinetics occurs between species **III** and **IV** (Figure 8), which significantly influences the reaction rates of **Ru1** and **Ru2**. In this step, the nitrogen atom in the Schiff-base ligand, which is coordinated to the metal center, undergoes dissociation. This dissociation reduces the coordination number of the metal center, leading to the formation of a 16-electron ($16e^-$) intermediate. The transition state corresponding to the formation of this species is estimated to be 92. 8 kJ/mol from species **III**, suggesting substantial kinetic hinderance. This $16e^-$ species is inherently less stable and hence is highly reactive as it undergo addition with additional ligand in the forthcoming step. The metal center in the $16e^-$ species establishes a strong η^2 interaction with the carbonyl (C=O) group of the aldehyde without any energy barrier. This interaction facilitates the reorganization of the system, ultimately forming species **IV**.

Natural Bond Orbital (NBO) analysis offers a detailed understanding of the charge distribution and the differential reactivity observed between the monometallic (**Ru2**) and bimetallic (**Ru1**) species. Specifically, the NBO analysis reveals differences in the natural charges on the nitrogen atom in the $16e^-$ species. In **Ru1**, the nitrogen carries a natural charge of −0.203/−0.201, while in **Ru2**, the nitrogen bears a slightly more negative charge of −0.211. This indicates that in **Ru1**, the charge is more delocalized across the ligand framework, suggesting a greater degree of electron sharing within the bimetallic system. The enhanced electronic distribution in **Ru1** promotes greater interaction between the metal center and the ligand, thereby accelerating the reaction. Additionally, computational studies demonstrate that the $16e^-$ intermediate in the bimetallic system is 44.5 kJ mol^{-1} more stable than the corresponding monometallic species. All these results indicate presence of cooperativity in **Ru1** and absence of the same in **Ru2** as the source of variation in the rate observed. This increased stability in the bimetallic complex further corroborates the experimentally observed trend of **Ru1** being more reactive, as the system is better stabilised and thus more readily participates in subsequent reaction steps. These findings are in agreement with experimental observations, highlighting the complementary nature of the bimetallic reactivity.

Detection of Ruthenium Hydride Species by NMR Spectroscopy

The presence of bulky 2,6-diisopropylphenyl groups in the vicinity of the metal center provides sufficient stability to the Ru–H species in the above mechanism, thus preventing its decomposition in the presence of oxygen. This is further supported by ex-situ NMR experiments on the Ru–H species (vide infra), which demonstrates its stability under the catalysis conditions.

An NMR experiment was conducted to detect ruthenium hydride in a reaction mixture. The NMR tube was prepared with **Ru1** (0.2 mmol), 0.4 mL of deuterated water, and 0.3 mL of buffer (pH 3.5). The mixture was heated at 60 °C for 15 minutes. Analysis with ^{1}H NMR spectroscopy revealed a characteristic peak at δ −7.87 ppm, indicating the presence of a Ru-hydride species (Figures 9 and S15). A color change from pale yellow to dark brown was also observed, suggesting the conversion of **Ru1** to the Ru-hydride intermediate.

To further investigate the formation of ruthenium hydride in **Ru1** and **Ru2** using other hydride sources, a controlled experiment was performed with sodium hydride in deuterated methanol following a similar procedure. The reaction mixtures were monitored using NMR and ESI-MS spectroscopy (Figure 10). In the ^{1}H NMR spectra, hydride peaks were detected at δ −7.39 ppm for **Ru1** (Figure S15) and δ −7.37 ppm for **Ru2** (Figure S17). ESI-MS confirmed the formation of ruthenium hydride in both cases, showing intense peaks at m/z 1031.32 corresponding to $[M–H]^+$ for the **Ru1** mixture and m/z 556.07 corresponding to $[M+K]^+$ for the **Ru2** mixture (Figures S18 and S19).

Conclusions

We have successfully performed highly effective and chemoselective TH of aldehydes in water with Ru(II) catalysts using formic acid/formate buffer as a hydride source. Aromatic,

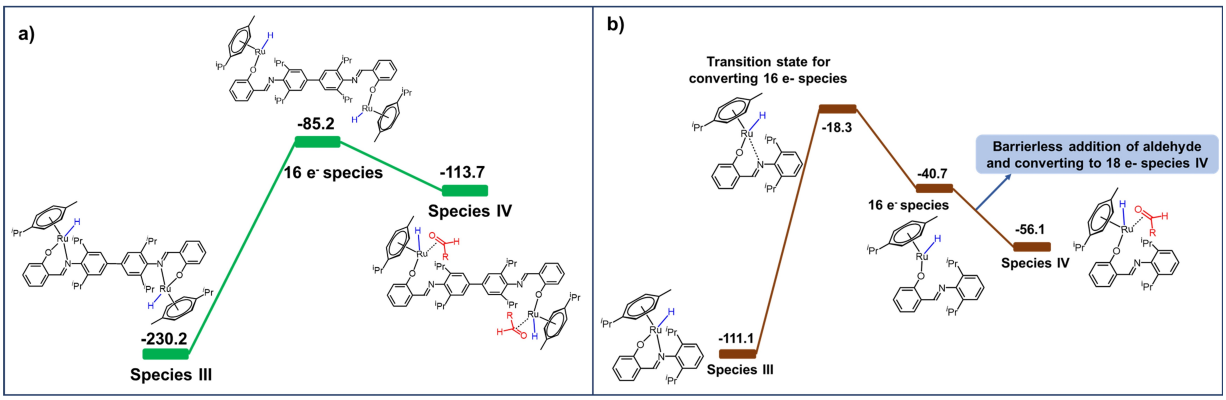

Figure 8. The comparison of kinetics for rate determining step of reaction, computed at the B3LYP–D3/def2-TZVP level of theory for **Ru1 (a)** and **Ru2 (b).**

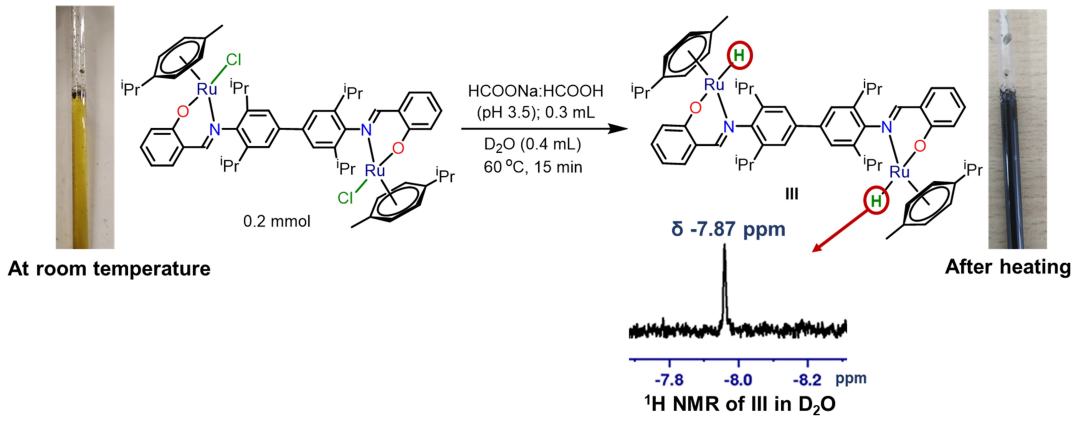

Figure 9. Detection of ruthenium hydride species using ^{1}H NMR spectroscopy.

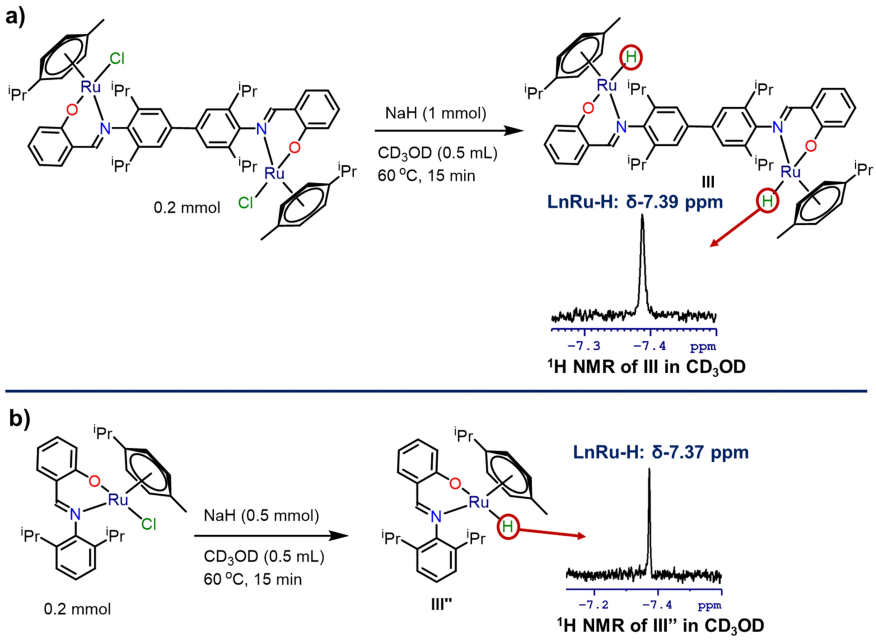

Figure 10. Detection of ruthenium hydride species using NMR and ESI-MS. a) reaction of **Ru1** with NaH and b) **Ru2** with NaH in CD_3OD.

aliphatic, and α, β-unsaturated aldehydes undergo selective TH reaction efficiently under mild reaction conditions with a catalyst loading of as low as 0.01 mol%. The catalyst was reused multiple times (till the 6th cycle) in consecutive cycles without sacrificing its efficiency. **Ru1** catalyst is remarkably effective, achieving highest TOFs value of $5.5 \times 10^5\ h^{-1}$ with 0.0001 mol% catalyst loading. Additionally, green metrics analyses revealed high atom economy (98.1%), atom efficiency (94.2%) and reaction mass efficiency (98%), demonstrating the TH in water with **Ru1** catalyst is an atom-efficient method. This method can also be used for large scale conversion since it operates under moderate reaction conditions with high chemo-selectivity and enhanced safety (no gaseous H_2). Detailed DFT calculation were performed to understand the mechanism of TH and also to probe the faster reactivity of **Ru1** compared to other catalyst. The result hint at the action of cooperativity being one of the reasons for enhanced reactivity for the dinuclear catalyst.

Experimental Section

Materials

Starting materials such as 2,2′,6,6′-tetraisopropylbenzidine (TIBZ),[43] Schiff base ligands $\mathbf{H_2L^1}$, $\mathbf{HL^2}$,[44,45] [Ru(*p*-cymene)(μ-Cl)Cl]$_2$,[46] and complexes **Ru1**,[37] **Ru2**[37] were prepared according to the reported procedures. Ruthenium(III)trichloride trihydrate, α-phellandrene, salicylaldehyde and 5-bromosalicylaldehyde (Sigma Aldrich), bromine (Spectrochem), 2,6-diisopropylaniline (Alfa Aesar), and benzaldehyde (Spectrochem) were used as received. Other substrates and analytical grade solvents were procured commercially and used without further purification. The ruthenium compounds reported herein are air and moisture-stable.

Physical Measurements and Instruments

All the experiments including catalyst synthesis and catalysis reaction were carried out in a well-ventilated fume hood under air. ^{1}H and ^{13}C NMR spectra were recorded on a Bruker AV III 400 MHz

NMR spectrometer using $CDCl_3$, D_2O and CD_3OD as solvent. Melting points were measured in glass capillaries and are reported uncorrected. FT-IR spectra were recorded on a PerkinElmer Spectrum One Infrared Spectrometer (Model number 73465) as KBr diluted discs in the frequency range 4000–400 cm^{-1}. Elemental analyses were performed on a Vario Micro Cube (Elemental Analysensysteme GmbH) microanalyzer. ESI-MS measurements were performed on a Bruker Maxis Impact electrospray mass spectrometer. UV-NIR-3600 spectrophotometer from Shimadzu was used for the UV-visible studies. An Agilent 7890 A GC system with an FID detector and a J & W DB-1 column (10 m, 0.1 mm ID) was used to conduct GC-MS analysis. Suitable single crystals of H_2L^3 and **Ru3** were grown directly from the crude products for X-ray diffraction analysis. Low-temperature single crystal X-ray diffraction intensity data were collected using a BRUKER D8 QUEST diffractometer equipped with an IμS DIAMOND microfocus Mo–Kα radiation source (λ = 0.71073 Å).[47–50] The elemental analyses report of H_2L^3 and **Ru3** were provided in the supporting information (Figures S23 and S24).

Computational Details

All DFT calculations have been performed in the Gaussian16.C suite of programs.[51] The methodology that has been used is B3LYP–D3 functional along with the basis set SDD for Ru atoms and 6–31G*[52,53] for other atoms. This is a time-tested methodology for the Ru catalyst and also has reproduced several experimental spectral features,[54] offering confidence in the methodology. The single point energies were computed on the optimized geometries with the def2-TZVP basis set for all atoms.[55] The Gibbs free energy correction has been added to the single point energies obtained from the higher basis set to refine the gas phase electronic energies. The solvation has been modeled using the polarisable continuum model (PCM), using water as the solvent.[56]

Synthesis of 2,2′-((1E,1′E)-((3,3′,5,5′-tetraisopropyl-[1,1′-biphenyl]-4,4′ diyl)bis(azaneyly lidene))bis(methaneylylidene))bis(4-bromophenol) (H_2L^3)

In round bottom flask, TIBZ (1.12 g, 3.2 mmol) was dissolved in methanol (100 mL). To this solution, 5-bromo salicylaldehyde (1.29 g, 6.4 mmol) and formic acid (5–6 drops) were added under stirring. The reaction mixture was refluxed for 12 hours to obtain a yellow precipitate. The yellow precipitate was collected by filtration and washed with cold methanol 2–3 times followed by crystallization from dichloromethane:methanol (5:1 v/v) mixtures to give pure H_2L^3 as yellow crystals. Yield (2.04 g, 88%). Mp. 266 °C. Anal. Cal. for $C_{38}H_{42}Br_2O_2N_2$; C, 63.52; H, 5.89; N, 3.90. Found: C, 63.13; H, 5.68; N, 3.39; ESI-MS: $[M+H]^+ = 719.166$ *m/z* (Mr = 718.574); ^{1}H NMR (400 MHz, $CDCl_3$) δ 13.41 (s, 2H), 8.31 (s, 2H), 7.53 (d, $^3J_{H,H} = 8.61$ Hz, 2H), 7.50 (s, 2H), 7.38 (s, 4H), 7.00 (d, $^3J_{H,H} = 8.65$ Hz, 2H), 3.04 (sept, $^3J_{H,H} = 6.85$ Hz, 4H), 1.27 (d, $^3J_{H,H} = 6.84$ Hz, 24H) ppm. ^{13}C NMR (101 MHz, $CDCl_3$) δ 165.59, 160.33, 145.01, 139.29, 139.08, 136.01, 134.30, 122.43, 120.06, 119.46, 110.62, 28.41, 23.61 ppm. FT-IR (KBr diluted pellet, cm^{-1}) 3380 (b), 2965 (s), 1628 (s), 1578 (s), 1426 (s), 1494 (w), 1470 (s), 1398 (s), 1322 (s), 1280 (s), 1238 (w), 1147 (s), 1112 (s), 913 (w), 872 (s), 761 (s), 681 (w). UV-Vis (dichloromethane, λ_{max} (nm), ε ($\times 10^5$ M^{-1} cm^{-1}); 234 (1.7), 271 (1.1), 348 (0.9).

Synthesis of [(*p*–cymene)$_2$(RuCl)$_2$L^3] (Ru3)

H_2L^3 (144 mg, 0.2 mmol)) and potassium carbonate (56 mg, 0.4 mmol) were mixed in ethanol (50 mL), to this mixture [Ru(*p*-cymene)(μ-Cl)Cl]$_2$ (122 mg, 0.20 mmol) was added under stirring. The colour of the reaction mixture changed from yellow to dark red indicating the progress of a reaction. The reaction mixture was stirred vigorously at room temperature overnight. After the completion of reaction, solvent was removed under vacuum, crude **Ru3** was obtained as dark red residue. The residue was dissolved in dichloromethane and filtered through celite. After solvent removal and recrystallization from dichloromethane:ethanol (4:1 v/v) mixture, **Ru3** was obtained in good yields. Yield (221 mg, 88%). Mp. decomposes at 210–212 °C. Anal. Cal. for $C_{58}H_{68}N_2O_2Cl_2Br_2Ru_2$; C, 55.37; H, 5.45; N, 2.23; Found: C, 54.99; H, 5.46; N, 2.17; ESI-MS: $[M-Cl]^+ = 1223.150$ (Mr = 1258.142); ^{1}H NMR (400 MHz, $CDCl_3$) 8.29 (s, 2H), δ 7.57 (s, 2H), 7.51 (d, $^3J_{H,H} = 9.01$ Hz, 2H), 7.21 (dd, $^3J_{H,H} = 9.01$ Hz, $^3J_{H,H} = 2.72$ Hz, 2H), 6.92 (d, $^3J_{H,H} = 2.96$ Hz, 2H), 6.84 (d, $^3J_{H,H} = 9.12$ Hz, 2H), 5.46 (d, $^3J_{H,H} = 6.10$ Hz, 2H), 5.36 (d, $^3J_{H,H} = 6.11$ Hz, 2H), 4.97 (d, $^3J_{H,H} = 6.14$ Hz, 2H), 4.33 (d, $^3J_{H,H} = 6.19$ Hz, 2H), 4.24 (sept, $^3J_{H,H} = 6.72$ Hz, 2H), 3.22 (sept, 6.97 Hz, 2H), 2.82 (sept, $^3J_{H,H} = 6.91$ Hz, 2H), 2.02 (s, 6H), 1.58 (d, $^3J_{H,H} = 6.73$ Hz, 6H), 1.48 (d, $^3J_{H,H} = 6.88$ Hz, 6H), 1.39 (d, $^3J_{H,H} = 6.84$ Hz, 6H), 1.30 (d, $^3J_{H,H} = 6.81$ Hz, 6H), 1.11 (d, $^3J_{H,H} = 6.93$ Hz, 12H) ppm. ^{13}C NMR (101 MHz, $CDCl_3$) δ 166.49, 165.81, 151.92, 143.20, 142.04, 140.06, 138.08, 136.06, 124.06, 123.04, 122.10, 120.91, 105.35, 104.67, 94.58, 87.88, 84.48, 82.03, 81.32, 80.55, 30.81, 28.10, 27.67, 26.86, 26.11, 23.39, 22.74, 22.41, 21.84, 17.899 ppm. FT-IR (KBr diluted pellet, cm^{-1}) 3001 (s), 1616 (s), 1493 (s), 1468 (s), 1390 (w), 1321 (s), 1235 (s), 1223 (s), 1164 (s), 1084 (w), 1025(s), 952, 746, 703 (s), 698 (w), 591 (s). UV-Vis (dichloromethane, λ_{max} (nm), ε ($\times 10^5$ M^{-1} cm^{-1})) 230 (2.1), 266 (1.5), 448 (45).

General Procedure for Hydrogenation of Aldehydes with Ru1

A flask containing a stir bar has been sequentially loaded with **Ru1** or **Ru3** (0.01 mol%) or **Ru2** (0.02 mol%), buffer solution (HCOONa: HCOOH, pH 3.5, 3 mL), and water (2.0 mL) and the resultant solution was stirred at 80 °C for 5 minutes. Aldehyde substrate (1 mmol) was then added to the reaction mixture, and the resulting mixture was stirred at 80 °C for 1 hour. GC-MS analysis was used to monitor the product formation. After completion of the reaction (under optimized conditions of 1 h at 80 °C), the product was extracted with ethyl acetate and dried over anhydrous sodium sulfate to obtain respective alcohols as pure products. The products have been further purified by column chromatography using petroleum ether - ethyl acetate mixture (98:2) as eluent. The products were analysed using NMR spectroscopy (see, ESI).

General Procedure for Reusing Catalyst Ru1

After the completion of the reaction, the resulting mixture was filtered, and most of the catalyst remained as a solid residue in the reaction flask. The catalyst was reused for the next catalytic run without further purification or activation.

Procedure for Aldehyde and Ketone Competitive Reaction

Ru1 (0.01 mol%, ~0.11 mg), buffer solution (HCOONa:HCOOH, pH 3.5, 3 mL), and water (2 mL) were added to a 10 mL round bottom flask and stirred at 80 °C for 5 minutes. Subsequently, an equimolar mixture of benzaldehyde (106 mg, 1 mmol) and acetophenone (120 mg, 1 mmol) was added, and the resulting reaction mixture was then stirred at 80 °C for 1 hour. After completion of the reaction, the product was extracted with ethyl acetate and dried over anhydrous sodium sulfate and was analysed by GC-MS spectrometry.

Acknowledgements

This work was supported by SERB, New Delhi through a J. C. Bose Fellowship grant to R. M. (SB/S2/JCB-85/2014). GR would like to acknowledge SERB for funding (CRG/2022/001697; SB/SJF/2019-20/12). G.D. thanks CSIR/UGC New Delhi and IIT Bombay for a research fellowship. TRKR acknowledges the financial support from the Prime Minister's Research Fellowship (PMRF). The authors thank the IoE-funded central facilities and SAIF, IIT Bombay for help with various spectral measurements.

Conflict of Interests

There are no conflicts to declare.

Data Availability Statement

The data that support the findings of this study are available in the supplementary material of this article.

Keywords: Bimetallic catalyst · Hydrogen transfer · Chemoselective · Ruthenium hydride

[1] G. J. Kelly, F. King, M. Kett, *Green Chem.* **2002**, *4*, 392–399.
[2] D. E. Ward, C. K. Rhee, *Synth. Commun.* **1988**, *18*, 1927–1933.
[3] X. Tan, G. Wang, Z. Zhu, C. Ren, J. Zhou, H. Lv, X. Zhang, L. W. Chung, L. Zhang, X. Zhang, *Org. Lett.* **2016**, *18*, 1518–1521.
[4] S. S. Kotha, N. Sharma, G. Sekar, *Adv. Synth. Catal.* **2016**, *358*, 1694–1698.
[5] S. E. Varjosaari, V. Skrypai, S. M. Herlugson, T. M. Gilbert, M. J. Adler, *Tetrahedron Lett.* **2018**, *59*, 2839–2843.
[6] P. Melle, J. Thiede, D. A. Hey, M. Albrecht, *Chem. Eur. J.* **2020**, *26*, 13226–13234.
[7] C. Romain, S. Gaillard, M. K. Elmkaddem, L. Toupet, C. Fischmeister, C. M. Thomas, J. L. Renaud, *Organometallics* **2010**, *29*, 1992–1995.
[8] J. Hannedouche, G. J. Clarkson, M. Wills, *J. Am. Chem. Soc.* **2004**, *126*, 986–987.
[9] D. Wang, D. Astruc, *Chem. Rev.* **2015**, *115*, 6621–6686.
[10] A. H. Aboo, E. L. Bennett, M. Deeprose, C. M. Robertson, J. A. Iggo, J. Xiao, *Chem. Comm.* **2018**, *54*, 11805–11808.
[11] H. Chai, Q. Wang, T. Liu, Z. Yu, *Dalton Trans.* **2016**, *45*, 17843–17849.
[12] A. Indra, P. Maity, S. Bhaduri, G. K. Lahiri, *ChemCatChem* **2013**, *5*, 322–330.
[13] M. M. Sheeba, M. M. Tamizh, L. J. Farrugia, A. Endo, R. Karvembu, *Organometallics* **2014**, *33*, 540–550.
[14] P. Dubey, S. Gupta, A. K. Singh, *Organometallics* **2019**, *38*, 944–961.
[15] G. Zhang, B. L. Scott, S. K. Hanson, *Angew. Chem. Int. Ed.* **2012**, *51*, 12102–12106.
[16] D. S. Mérel, M. Elie, J. F. Lohier, S. Gaillard, J. L. Renaud, *ChemCatChem* **2013**, *5*, 2939–2945.
[17] T. Abura, S. Ogo, Y. Watanabe, S. Fukuzumi, *J. Am. Chem. Soc.* **2003**, *125*, 4149–4154.
[18] S. Ogo, N. Makihara, Y. Watanabe, *Organometallics* **1999**, *18*, 5470–5474.
[19] Y. Wei, D. Xue, Q. Lei, C. Wang, J. Xiao, *Green Chem.* **2013**, *15*, 629–634.
[20] X. Wu, X. Li, A. Z. Gerosa, A. Pettman, J. Liu, A. J. Mills, J. Xiao, *Chem. Eur. J.* **2008**, *14*, 2209–2222.
[21] D. Talwar, X. Wu, O. Saidi, N. P. Salguero, J. Xiao, *Chem. Eur. J.* **2014**, *20*, 12835–12842.
[22] X. Wu, X. Li, F. King, J. Xiao, *Angew. Chem., Int. Ed.* **2005**, *44*, 3407–3411.
[23] X. Wu, J. Liu, X. Li, A. Z. Gerosa, F. Hancock, D. Vinci, J. Ruan, J. Xiao, *Angew. Chem., Int. Ed.* **2006**, *45*, 6718–6722.
[24] X. Wu, C. Corcoran, S. Yang, J. Xiao, *ChemSusChem* **2008**, *1*, 71–74.
[25] J. T. Liu, S. Yang, W. Tang, Z. Yang, J. Xu, *Green Chem.* **2018**, *20*, 2118–2124.
[26] N. Luo, J. Liao, L. Ouyang, H. Wen, J. Liu, W. Tang, R. Luo, *Organometallics* **2019**, *38*, 3025–3031.
[27] Z. Yang, Z. Zhu, R. Luo, X. Qiu, J. T. Liu, J. K. Yang, W. Tang, *Green Chem.* **2017**, *19*, 3296–3301.
[28] V. Diachenko, M. J. Page, M. R. D. Gatus, M. Bhadbhade, B. A. Messerle, *Organometallics* **2015**, *34*, 4543–4552.
[29] H. Fujita, S. Takemoto, H. Matsuzaka, *ACS Catal.* **2021**, *11*, 7460–7466.
[30] H. F. Yuen, T. J. Marks, *Organometallics* **2009**, *28*, 2423–2440.
[31] M. E. Broussard, B. Juma, S. G. Train, W. J. Peng, S. A. Laneman, G. G. Stanley, *Science* **1993**, *260*, 1784–1788.
[32] H. Chai, Q. Wang, T. Liu, Z. Yu, *Dalton Trans.* **2016**, *45*, 17843–17849.
[33] Y. Nishibayashi, A. Shinoda, Y. Miyake, H. Matsuzawa, M. Sato, *Angew. Chem., Int. Ed.* **2006**, *45*, 4835–4839.
[34] S. C. Ammal, N. Yoshikai, Y. Inada, Y. Nishibayashi, E. Nakamura, *J. Am. Chem. Soc.* **2005**, *127*, 9428–9438.
[35] H. Chai, Q. Wang, T. Liu, Z. Yu, *Dalton Trans.* **2016**, *45*, 17843–17849.
[36] H. Chai, T. Liu, D. Zheng, Z. Yu, *Organometallics* **2017**, *36*, 4268–4277.
[37] G. Deshmukh, T. R. K. Rana, N. Yadav, G. Rajaraman, R. Murugavel, *Green Chem.* **2024**, *26*, 1610–1626.
[38] G. Deshmukh, S. J. Gharpure, R. Murugavel, *Organometallics* **2024**, *43*, 1190–1202.
[39] G. Deshmukh, R. Murugavel, *Eur. J. Org. Chem.* **2024**, *27*, e202400131.
[40] G. Deshmukh and R. Murugavel, *Synlett* **2024**, DOI: 10.1055/a-2294-1643.
[41] X. J. Yun, C. Ling, W. Deng, Z. J. Liu, Z. J. Yao, *Organometallics* **2020**, *39*, 3830–3838.
[42] C. Wang, C. Li, X. Wu, A. Pettman, J. Xiao, *Angew. Chem., Int. Ed.* **2009**, *48*, 6524–6528.
[43] P. Wehrmann, S. Mecking, *Organometallics* **2008**, *27*, 1399–1408.
[44] R. Jangir, D. Kaleeswaran, R. Murugavel, *ChemistrySelect* **2018**, *3*, 8082–8094.
[45] R. Jangir, M. Ansari, D. Kaleeswaran, G. Rajaraman, M. Palaniandavar, R. Murugavel, *ACS Catal* **2019**, *9*, 10940–10950.
[46] M. A. Bennett, T. N. Huang, T. W. Matheson, A. K. Smith, S. Ittel, W. Nickerson, *Inorg. Synth.* **1982**, *21*, 74–78.
[47] CrysAlisPRO, Oxford Diffraction/Agilent Technol. UKLtd, Yarnton, Oxford, UK, **2014** .
[48] L. J. Farrugia, *J. Appl. Crystallogr.* **2012**, *45*, 849–854.
[49] O. V. Dolomanov, L. J. Bourhis, R. J. Gildea, J. A. K. Howard, H. Puschmann, *J. Appl. Crystallogr.* **2009**, *42*, 339–341.
[50] G. M. Sheldrick, *Acta Crystallogr., Sect. C: Struct. Chem.* **2015**, *71*, 3–8.
[51] M. J. Frisch, G. W. Trucks, H. B. Schlegel, G. E. Scuseria, M. A. Robb, J. R. Cheeseman, G. Scalmani, V. Barone, G. A. Petersson, H. Nakatsuji, X. Li, M. Caricato, A. V. Marenich, J. Bloino, B. G. Janesko, R. Gomperts, B. Mennucci, H. P. Hratchian, J. V. Ortiz, A. F. Izmaylov, J. L. Sonnenberg, D. Williams-Young, F. Ding, F. Lipparini, F. Egidi, J. Goings, B. Peng, A. Petrone, T. Henderson, D. Ranasinghe, V. G. Zakrzewski, J. Gao, N. Rega, G. Zheng, W. Liang, M. Hada, M. Ehara, K. Toyota, R. Fukuda, J. Hasegawa, M. Ishida, T. Nakajima, Y. Honda, O. Kitao, H. Nakai, T. Vreven, K. Throssell, J. A. Montgomery Jr., J. E. Peralta, F. Ogliaro, M. J. Bearpark, J. J. Heyd, E. N. Brothers, K. N. Kudin, V. N. Staroverov, T. A. Keith, R. Kobayashi, J. Normand, K. Raghavachari, A. P. Rendell, J. C. Burant, S. S. Iyengar, J. Tomasi, M. Cossi, J. M. Millam, M. Klene, C. Adamo, R. Cammi, J. W. Ochterski, R. L. Martin, K. Morokuma, O. Farkas, J. B. Foresman, D. J. Fox, *Gaussian 16, Revision C.01*, Gaussian, Inc., Wallingford CT **2016**.
[52] R. Ditchfield, W. J. Hehre, J. A. Pople, *J. Chem. Phys.* **1971**, *54*, 720–723.
[53] P. J. Hay, W. R. Wadt, *J. Chem. Phys.* **1985**, *82*, 299–310.
[54] S. Kumar, Ta, C. Nettem, J. M. Tanski, G. Rajaraman, P. Ghosh, *RSC Adv.* **2022**, *12*, 28961–28984.
[55] F. Weigend, R. Ahlrichs, *Phys. Chem. Chem. Phys.* **2005**, *7*, 3297–3305.
[56] J. Tomasi, B. Mennucci, R. Cammi, *Chem. Rev.* **2005**, *105*, 2999–3093.

Manuscript received: September 10, 2024
Revised manuscript received: November 11, 2024
Accepted manuscript online: November 12, 2024
Version of record online: November 29, 2024